A Simplified Model of the Effect of a Fire Sprinkler Spray on a Buoyant Fire Plume

JOHN A. SCHWILLE AND RICHARD M. LUEPTOW*

Department of Mechanical Engineering
Northwestern University
2145 Sheridan Road, Evanston, IL 60208, USA

ABSTRACT: Equations describing the fluid motion in buoyant plumes have been applied to fire plumes by researchers and engineers since Morton et al. developed them in the 1950s. However, in the application of active fire suppression by water droplets, the equations are no longer valid. The equations have been modified to include the effect of a homogeneous, uniform velocity droplet field on the momentum of the fluid. Solving the resulting ordinary differential equations shows that the plume widens and the upward velocity of the plume slows significantly due to the presence of droplets. Results from this simple model appear to match the results of more sophisticated numerical simulations. The model further demonstrates that the interaction between the upward momentum of the plume and the downward momentum of the droplet spray can be critical for fire suppression.

KEY WORDS: sprinkler spray, fire plume, fire suppression, droplet momentum, suppression model.

INTRODUCTION

EVEN WITH EFFORTS to reduce fire hazards, fire continues to pose a significant threat to people and property. Fire causes over 3000 accidental deaths each year in the United States [1], and it has been estimated that the cost of fire to developed nations is about 1% of their gross domestic product each year [2]. Automatic fire sprinklers are extremely effective in reducing these losses.

The environment for a fire sprinkler is shown in Figure 1. Combustion occurs in the luminous flame region. The hot products of this combustion are less dense than the surrounding air and rise, creating a buoyant plume.

*Author to whom correspondence should be addressed. E-mail: r-lueptow@northwestern.edu

1042-3915/06/02 0131–23 $10.00/0 DOI: 10.1177/1042391506056001

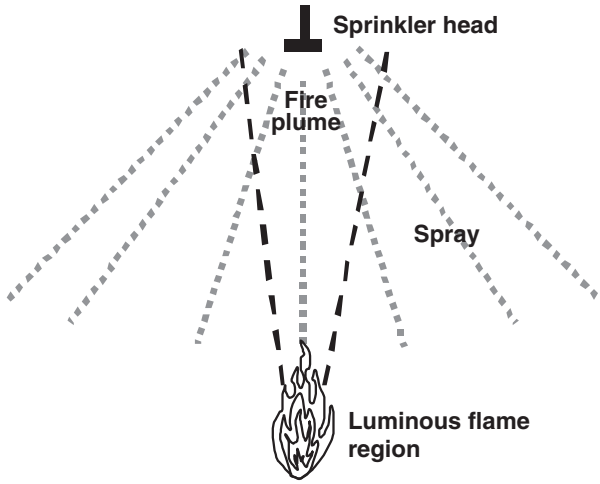

Figure 1. *The fire sprinkler environment.*

If the fire occurs in a sprinklered facility, the hot gases will eventually transfer enough energy to the fire sprinkler's heat-sensitive element for activation and release of water. The stream of water issuing from the orifice of the sprinkler is formed into a spray by a deflector. As shown schematically, the droplets in the spray travel down through the hot plume to suppress the fire.

The droplets from fire sprinklers prevent and suppress fires through four physical mechanisms: direct cooling of the burning surface, oxygen displacement through evaporation, evaporative cooling, and preventing flame spread by prewetting surrounding surfaces. For any of these mechanisms, penetration of the droplet spray into the fire plume is essential.

Significant work has been carried out in both flames and generic sprays individually, and the work has been the subject of reviews [3–5]. However, little research has been performed focusing on the interaction between the fire and the fire sprinkler spray. Understanding the interaction between the downward moving droplet spray and the upward buoyant plume is crucial to improving fire suppression efforts.

For a fire and the resulting plume without a spray, researchers and engineers have successfully used the equations for a buoyant plume to predict the plume width, plume velocity, and plume temperature for many years. The majority of these correlations stem from the theory by Morton et al. for buoyant plumes [6]. However, these equations for the hot plume do not account for the spray from a fire sprinkler. Experimental results indicate that droplets falling from a fire sprinkler interact with the upward buoyant plume and significantly change the nature of the flow field [7].

Recently, computational fluid dynamics (CFD) models have been developed that combine droplet spray computations with numerical solutions to the Navier–Stokes equations for the plume flow. Nam [8,9] developed a model to simulate a fire sprinkler spray interacting with a fire plume using a Eulerian approach for the gaseous phase and a Lagrangian particle tracking method for the droplet spray. The results from this model show a well-defined boundary between the downward moving air entrained by the sprinkler droplets and the upward moving thermal plume, referred to as the 'interaction region.' In another computational approach, a large-eddy simulation code for modeling buoyancy-dominated flows, known as the fire dynamics simulator (FDS) [10], has been developed to model fires and fire suppression. Recently, experimental measurements of sprinkler sprays [11] have been incorporated into the code. Thus, there are several tools that can be used to predict fire scenarios. However, these models do not necessarily provide insight into the physics of the interaction between the upward buoyant plume and the falling droplets because of their complexity. Consequently, a simple model is proposed that isolates one interaction mechanism to better understand the competition between the plume and the droplets. In this article, the equations for a buoyant plume developed by Morton et al. [6] are modified to include the effect of a droplet spray. The resulting model characterizes the interaction between the downward momentum of the spray and the upward momentum of the plume. The model is quite simple and is not intended to simulate all the details of the interaction between the plume and the droplets. Instead, the purpose of the model is to better understand this interaction. In effect, if the momentum of the spray overcomes the momentum of the plume, droplets are delivered to the flaming region and the fire is suppressed. Otherwise the fire may continue to grow.

MODEL

In their original analysis, Morton et al. makes four assumptions regarding a buoyant plume:

- The plume is assumed to originate from a point source.
- The rate of air entrainment into the plume is assumed to be proportional to the plume velocity at that height.
- The profiles of the mean vertical velocity and the mean buoyant force at different heights above the source are similar.
- The variations of density in the field of motion are assumed to be small compared to the ambient density.

These assumptions appear to be generally valid for fire plumes, so the Morton analysis is the standard basis for many fire correlations [12].

From the assumptions above, Morton et al. [6] derived conservation equations for volume, momentum, and density deficiency (buoyancy) in a buoyant plume.

$$\frac{\mathrm{d}(b^2u)}{\mathrm{d}z} = 2\alpha bu \tag{1}$$

$$\frac{\mathrm{d}(b^2u^2)}{\mathrm{d}z} = b^2g\frac{\rho_1 - \rho}{\rho_1} \tag{2}$$

$$\frac{\mathrm{d}}{\mathrm{d}z}\left(b^2ug\frac{\rho_1 - \rho}{\rho_1}\right) = 0 \tag{3}$$

Following the standard Morton method and notation, b, u, and ρ indicate plume width, vertical velocity, and density, respectively, all of which are functions of the vertical distance, z, from the plume source at $z=0$. In addition, g is the acceleration due to gravity, ρ_1 is the density of the ambient air, and α is the entrainment coefficient, or the fraction of the plume velocity corresponding to the velocity of the ambient air being entrained into the plume. In Equation (3), density is considered to be a passive scalar that is conserved in a similar manner to species concentration in a mixing problem.

If a droplet spray is interacting with the buoyant plume, the momentum Equation (2) must be adjusted to account for the downward drag force the droplets exert on the upward plume. Consider the general form of the steady integral momentum conservation equation, which is

$$\sum \boldsymbol{F} = \int_{cv} \rho \boldsymbol{v}(\boldsymbol{v}\cdot\boldsymbol{n})\,\mathrm{d}A \tag{4}$$

where $\boldsymbol{F}$ represents the forces on the air, $\boldsymbol{v}$ is the air velocity, $\boldsymbol{n}$ is the unit normal, and $\mathrm{d}A$ is the differential area. The two vertical forces acting on the air are the upward buoyant force due to the difference in density between the plume and the ambient, and the downward drag force on the air due to the difference in droplet velocity and plume velocity. Using the disk-shaped elemental control volume in Figure 2, the buoyant force is

$$\mathrm{d}F_\mathrm{B} = (\rho_1 - \rho)g\pi b^2\mathrm{d}z \tag{5}$$

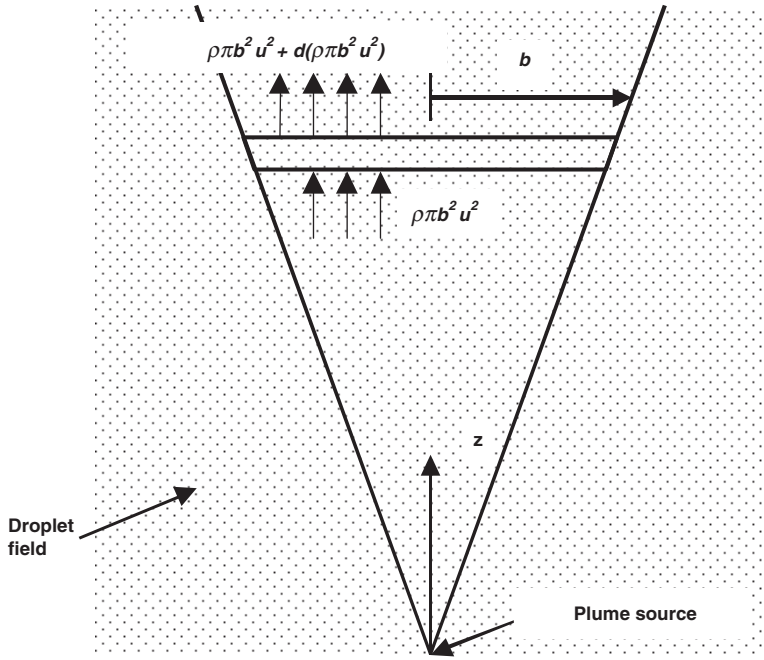

Figure 2. *Representation of a buoyant plume with a uniform droplet spray. The momentums into and out of a disk-shaped elemental control volume of radius b are shown.*

The vertical drag force on the plume due to the droplets in the elemental volume can be expressed as

$$\mathrm{d}F_{\mathrm{D}} = n\left[\frac{1}{2}C_{\mathrm{d}}\rho A_{\mathrm{d}}(u-u_{\mathrm{d}})|u-u_{\mathrm{d}}|\right](\pi b^2\,\mathrm{d}z) \tag{6}$$

where u_{d} is the vertical droplet velocity, C_{d} is the drag coefficient, A_{d} is the droplet's cross-sectional area and n is the number density of droplets. The bracketed term in Equation (6) represents the drag due to a single droplet, while $n\pi b^2\,\mathrm{d}z$ gives the total number of droplets in the control volume. It is assumed that the droplet velocity is vertical, a reasonable assumption at a short distance below the sprinkler [13]. The drag coefficient, C_{d} can be calculated as function of the Reynolds number,

$$\mathrm{Re} = \frac{2|u-u_{\mathrm{d}}|}{\nu}\sqrt{\frac{A_{\mathrm{d}}}{\pi}} \tag{7}$$

such that [14]

$$C_d = \begin{cases} \dfrac{24}{\mathrm{Re}}(1 + 0.15\,\mathrm{Re}^{0.687}) & \mathrm{Re} < 1000 \\ 0.44 & \mathrm{Re} > 1000 \end{cases} \tag{8}$$

Substituting into Equation (4) in accordance with the vertical forces and momentum for the disk-shaped elemental control volume in Figure 2, gives the result

$$-\mathrm{d}F_D + \mathrm{d}F_B = \mathrm{d}\,(\rho\pi b^2 u^2) \tag{9}$$

having assumed a uniform profile for plume velocity, just as Morton et al. did.

It is assumed that the momentum of the droplets entering the control volume is the same as that leaving the control volume, so these terms do not enter the right-hand side of Equation (9). This assumption is justified on the following basis. Measurements of the velocity of a fire sprinkler spray indicate that droplets fall at approximately their terminal velocity [13,15]. Furthermore, the largest volume of water carried in the spray is carried by the largest droplets [11], the size of which is altered least by evaporation. Thus, to a first approximation, the assumption that the momentum of the droplets does not significantly change is reasonable.

Assuming that density variations are small and simplifying, Equation (9) takes the form of a modified version of Morton's conservation of momentum

$$\frac{\mathrm{d}\,(b^2u^2)}{\mathrm{d}z} = b^2 g \frac{\rho_1 - \rho}{\rho_1} - \frac{b^2 n[C_d A_d (u - u_d)|u - u_d|]}{2} \tag{10}$$

The second term on the right-hand side accounts for the droplet spray reducing the momentum of the upward plume.

Equations (1), (3), and (10) form a set of modified plume equations. Inherent in these equations are the assumptions from the original analysis of Morton et al. plus the following assumptions:

- The droplet spray consists of uniform diameter droplets moving at a constant velocity (such as the terminal velocity) in the entire plume domain.
- The number density of droplets is uniform over the entire plume domain.

The consequence of these assumptions is that the momentum of the droplet spray does not change with z. Of course, in reality this is not true

since the momentum change in the plume is caused in part by momentum transfer from the droplets. However, given the assumptions of uniform plume velocity across the cross section and point source of buoyancy, this approximation is also reasonable.

The three boundary conditions for Equations (1), (3), and (10) are (1) the plume width at the source is zero ($b=0$), (2) the vertical momentum at the source is zero ($\rho u^2=0$), and (3) the weight deficiency is released by the point source at a known and constant rate $Q=b^2ug(\rho_1-\rho)/\rho_1$. For a fire plume, Q can be related to the heat release rate of the fire.

Morton's original equations have an analytical solution, but because of the non-linear drag term in Equation (10), the modified plume equations were solved numerically. The initial conditions were applied at one end point of the domain, and a fourth-order Runge-Kutta routine was used to numerically integrate the equations. By defining the gravity and density difference term that appears in the same form in Equations (3) and (10) as

$$\rho_{\mathrm{dif}}=g\left[\frac{(\rho_1-\rho)}{\rho_1}\right] \tag{11}$$

which will be called the buoyancy and defining the term for the drag on a single drop as:

$$\frac{1}{2}[C_{\mathrm{d}}\rho A_{\mathrm{d}}(u-u_{\mathrm{d}})|u-u_{\mathrm{d}}|]=\rho f_{\mathrm{D}} \tag{12}$$

Equations (1), (3), and (10) can be expressed in terms of first-order derivatives of the primary variables b, u, and ρ_{dif}:

$$\frac{\mathrm{d}b}{\mathrm{d}z}=2\alpha-\frac{b\rho_{\mathrm{dif}}}{2u^2}+\frac{bnf_{\mathrm{D}}}{2u^2} \tag{13}$$

$$\frac{\mathrm{d}u}{\mathrm{d}z}=-\frac{\rho_{\mathrm{dif}}}{u}-\frac{nf_{\mathrm{D}}}{u}-\frac{2\alpha u}{b} \tag{14}$$

$$\frac{\mathrm{d}}{\mathrm{d}z}(\rho_{\mathrm{dif}})=\frac{-2\alpha\rho_{\mathrm{dif}}}{b} \tag{15}$$

with the same initial conditions as the original Morton analysis. Thus, $b=0$, $\rho u^2=0$, and $b^2ug(\rho_1-\rho)/\rho_1=Q$ at the plume origin $z=0$.

The initial conditions create some difficulty in the numerical procedure, because several terms in the equations are indeterminate at $z=0$. To overcome this problem, assume the droplets' effect on the plume variables is negligible near the plume origin. The modified plume equations can then be

numerically solved based on initial conditions from Morton's original analytical solutions at a height $z = z_0$, which is set very close to the origin at $z = 0$:

$$b(z_0) = \frac{6\alpha}{5} z_0 \tag{16}$$

$$u(z_0) = \frac{5}{6\alpha}\left(\frac{9}{10}\alpha Q\right)^{1/3} z_0^{-1/3} \tag{17}$$

$$\rho_{\text{dif}}(z_0) = \frac{5Q}{6\alpha}\left(\frac{9}{10}\alpha Q\right)^{-1/3} z_0^{-5/3} \tag{18}$$

Using these initial conditions based on Morton's solution provides nonzero values for b for a very small z_0, thus preventing singularities in the equations.

To test this approach for the initial conditions, the sensitivity of the solution to the starting point, z_0, was investigated. Using reasonable values for n, u_d, Q, and d, and varying z_0 from 0.01 to 0.1 m resulted in changes in the calculated values of b, u, and ρ_{dif} of $< 0.05\%$ at a distance of 1 m above the origin and $< 0.02\%$ at a distance of 2 m above the origin. Thus, using initial conditions based on Morton's analysis with no droplets appears appropriate.

One further point is that the Morton solution and our variation on it result in unrealistic densities very near the origin. This is not a problem except in the calculation of the Reynolds number to determine the drag. To avoid this problem, the ambient density was used to calculate the Reynolds number, since throughout much of the plume the plume density is quite similar to the ambient density.

RESULTS

To begin, consider results for a case in which the global number density is $n = 500{,}000\ \text{drops/m}^3$ and the droplet velocity is $u_d = -4\ \text{m/s}$, respectively. These values are within the ranges seen in experiments for plumes and fire sprinklers [7]. The entrainment coefficient, α, has been set at 0.093, the value from the original Morton analysis. Q is set to $1\ \text{m}^4/\text{s}^3$, which is equivalent to a typical wastebasket fire of about 100 kW. Droplet sizes are typically 200 μm to 1.5 mm [11,16], so the droplet diameter was arbitrarily set to $d = 0.001$ m. Results are shown in Figure 3. From left to right, Figure 3 shows the effect of droplets on profiles of plume width (b), plume vertical

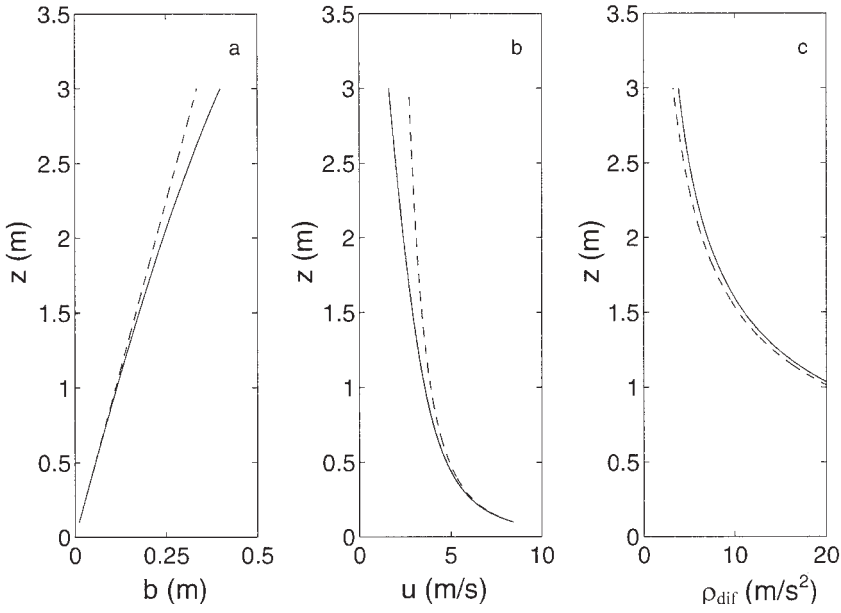

Figure 3. *The effect of droplets on plume variables for $n = 500{,}000$ drops/m^3, $u_d = -4$ m/s, $Q = 1$ m^4/s^3, and $d = 0.001$ m (dashed curve: plume with no droplets (Morton solution); solid curve: plume with droplets).*

velocity (u), and the buoyancy (ρ_{dif}) as a function of distance from the plume source (z). The plume origin is in the lower left corner of Figure 3(a). The solid curve shows the results of the analysis for a spray, while the dashed curve represents the results for the original Morton analysis with no spray. Figure 3(a) indicates that the spray slightly widens the plume compared to the original plume width, particularly far from the origin. A similar widening has been seen in a previous work using a two-dimensional k–ε CFD model [17]. In addition, the plume's vertical velocity decreases more with increasing z for the case with droplets than without droplets as shown in Figure 3(b). At 3 m above the plume origin, the upward plume velocity is a little more than half of what it would be with no spray. These results agree with the intuitive expectation that downward moving droplets would cause a slowing of upward plume velocity due to drag and a widening of the plume due to the net downward force of the droplets. The buoyancy shown in Figure 3(c) is slightly affected by the spray because of the widening of the plume, but it is very similar to the droplet-free plume's buoyancy. As discussed above, the large, nonphysical values of velocity and buoyancy near $z = 0$ are a result of the mathematical singularity at the origin, just as in Morton's original analysis.

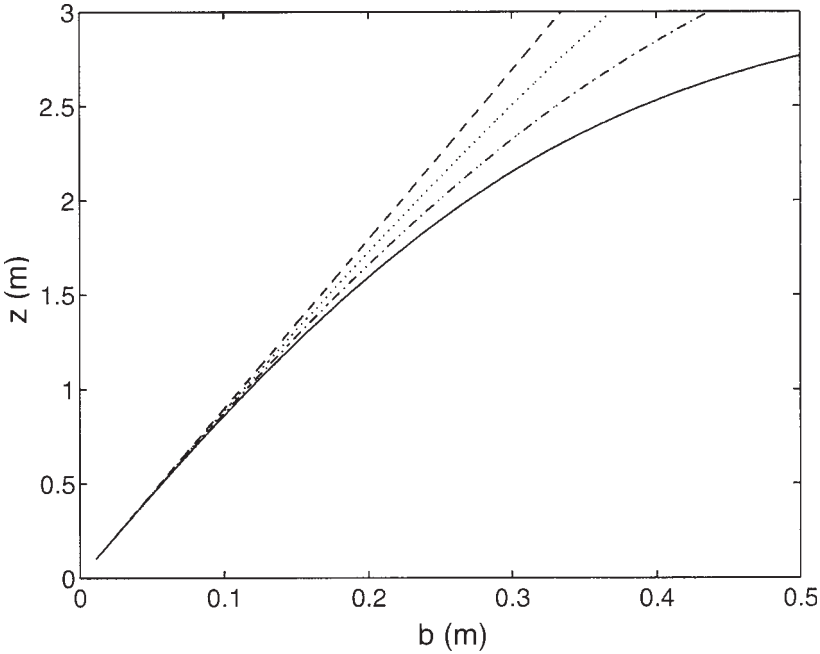

Figure 4. *The effect of droplet number density, n, on plume width, b with $Q = 1\,m^4/s^3$, $d = 0.001\,m$ and $u_d = -5\,m/s$ (dashed curve: $n = 1\,drop/m^3$; dotted curve: $n = 250{,}000\,drops/m^3$; dashed/dotted curve: $n = 500{,}000\,drops/m^3$; solid curve: $n = 750{,}000\,drops/m^3$).*

To further test the model, a sensitivity study was performed to determine the dependence of the model on the spray parameters n and u_d. Figure 4 shows the sensitivity of the plume width to the global number density, n. Profiles of plume width for four different values of n ranging from 1 drop/m^3 to 750,000 drops/m^3 are shown. Q, u_d, and d were held constant at 1 m^4/s^3, -5 m/s, and 0.001 m, respectively. It is clear that a very low number density would not affect the plume. As a result, the plume width for $n = 1$ matches the Morton solution, confirming that the numerical method has worked properly. As the number density is increased from 250,000 to 750,000 drops/m^3, the deviation of the plume width from the droplet-free plume becomes significant at large distances from the plume origin.

Figure 5 shows the sensitivity of the upward plume velocity to changes in number density. Again, the difference between Morton's unmodified solution and the calculations for $n = 1$ is negligible. However, the upward velocity of the plume is slowed significantly by the downward motion of the droplets as the number density is increased above 250,000 drops/m^3. In fact,

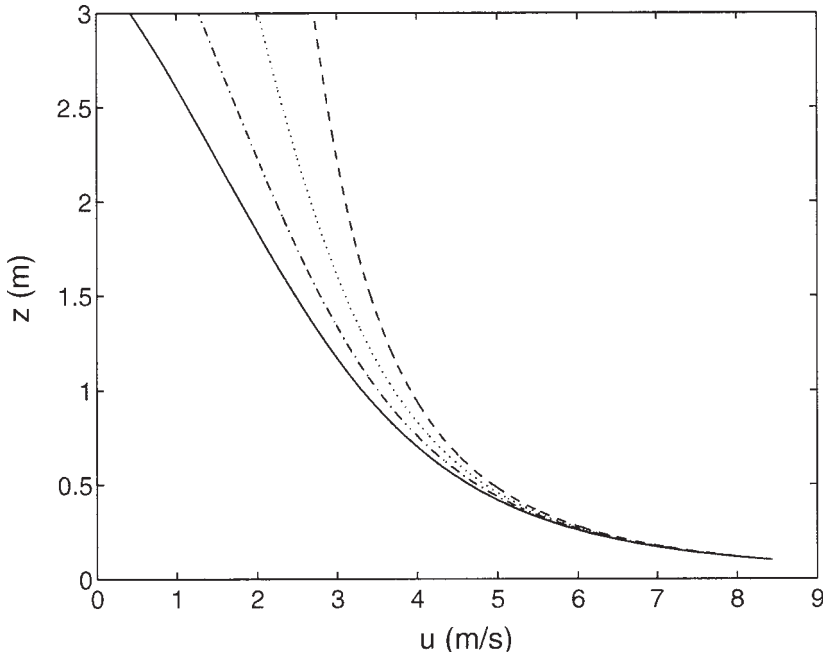

Figure 5. *The effect of droplet number density, n, on plume velocity, u, with $Q = 1\,m^4/s^3$, $d = 0.001\,m$, and $u_d = -5\,m/s$ (dashed curve: $n = 1\,drop/m^3$; dotted curve: $n = 250{,}000\,drops/m^3$; dashed/dotted curve: $n = 500{,}000\,drops/m^3$; solid curve: $n = 750{,}000\,drops/m^3$).*

by an elevation of 3 m, the upward velocity for $n = 750{,}000\,\text{drops/m}^3$ is only about 15% of what it would be with no spray.

The effect of increasing the downward drop velocity (u_d), shown in Figures 6 and 7, is similar to that of increasing the droplet number density. In this case, increasing u_d from 0 to $-5\,\text{m/s}$ leads to an increase in plume width and a decrease in plume velocity. Even when the droplets have zero downward velocity ($u_d = 0$), there is a small effect on the plume compared to Morton's solution because of the relative velocity between the upward plume and the downward droplets. It is clear that a more powerful downward spray (larger negative u_d) slows the upward plume significantly and causes it to broaden.

Of course, the analysis is also sensitive to the value for the entrainment coefficient, α, which prescribes the rate at which ambient air is entrained into the plume. Morton et al. suggest a value of $\alpha = 0.093$ based on experiments for a buoyant plume [6]. However, a variety of values for the entrainment coefficient have been proposed [18]. Low values ($\alpha = 0.057$)

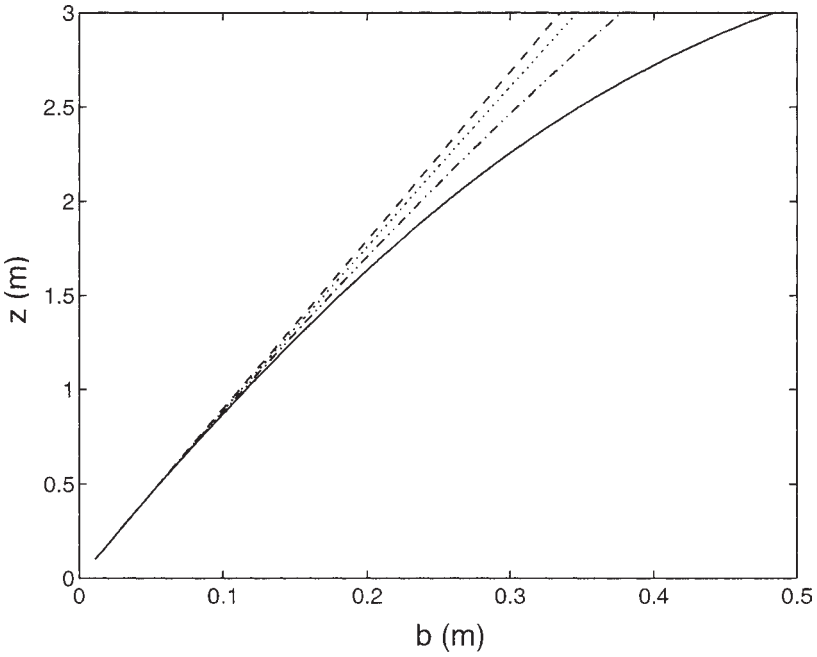

Figure 6. *The effect of droplet velocity, u_d, on plume width, b, with $Q = 1\,m^4/s^3$, $d = 0.001\,m$, and $n = 600{,}000\,drops/m^3$ (dashed curve: plume with no droplets (Morton solution); dotted curve: $u_d = 0\,m/s$; dashed/dotted curve: $u_d = -2.5\,m/s$; solid curve: $u_d = -5\,m/s$).*

correspond to jets while higher values correspond to plumes. The lowest consistently reported value for plumes is $\alpha = 0.082$. Hence, consider this as the lower bound for this sensitivity analysis. The highest value is more difficult to estimate. However, a reasonable relation for the entrainment coefficient is $\alpha = 0.057 + 0.097/\mathrm{Fr}$, where Fr is the Froude number [18]. Based on this relation, the entrainment value proposed by Morton et al. corresponds to $\mathrm{Fr} = 2.69$. If it is assumed that the Froude number could be reduced by half, then the corresponding entrainment coefficient is $\alpha = 0.129$. Thus, consider the dependence of the plume width, plume velocity, and plume density over the entire range of possible values for the entrainment coefficient (from $\alpha = 0.082$ to 0.129) in Figure 8. It is clear from the deviation of these quantities from that for $\alpha = 0.093$ that the entrainment coefficient plays a role in the model. However, the deviation is small given that the full range of reasonable values for the entrainment coefficient are shown in Figure 8. Thus, the model appears to be relatively insensitive to the specific value for α.

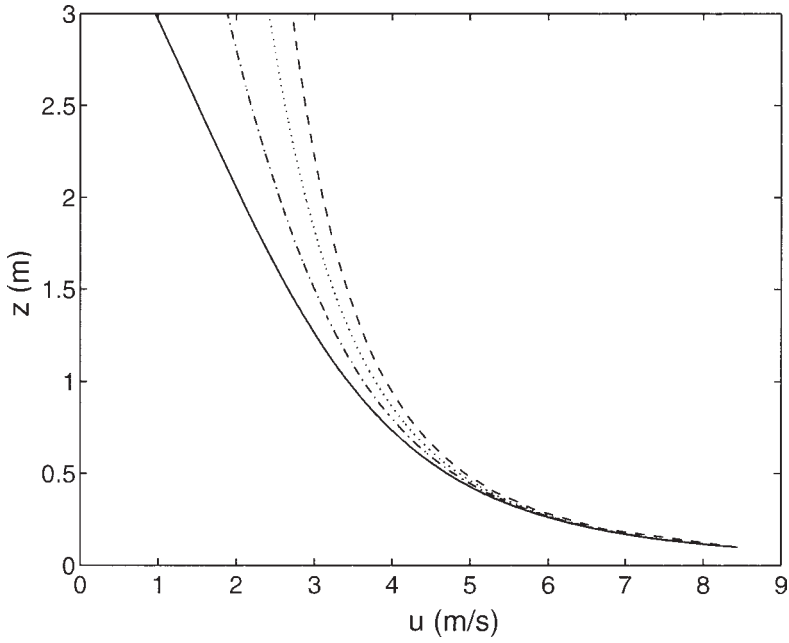

Figure 7. *The effect of droplet velocity, u_d, on plume velocity, u, with $Q = 1\,m^4/s^3$, $d = 0.001\,m$, and $n = 600{,}000\,drops/m^3$ (dashed curve: plume with no droplets (Morton solution); dotted curve: $u_d = 0\,m/s$; dashed/dotted curve: $u_d = -2.5\,m/s$; solid curve: $u_d = -5\,m/s$).*

In fire suppression, one might think of the situation as a competition between the upward momentum of the fire plume and the downward momentum of the spray. If the spray has a very large momentum, it will penetrate the plume and suppress the fire. If, instead, the momentum of the fire plume dominates, the spray is unlikely to penetrate the fire and the fire will grow. To quantify the competition in momentum between the plume and the spray, consider the height above the fire where the plume velocity goes to zero as a result of the downward drag of the droplets. If the spray is strong enough that the plume velocity goes to zero very near the fire origin, the fire should be suppressed. However, if the fire is strong enough so that its vertical velocity does not decrease to zero until far above the fire, the fire should grow. In terms of the analysis presented here, for a given combination of n and u_d, there is a vertical position, called the 'interaction boundary,' z_b, where the upward plume momentum balances the downward spray momentum. At this position, the plume velocity goes to zero and the plume widens rapidly. Figure 9 shows an example where the vertical velocity

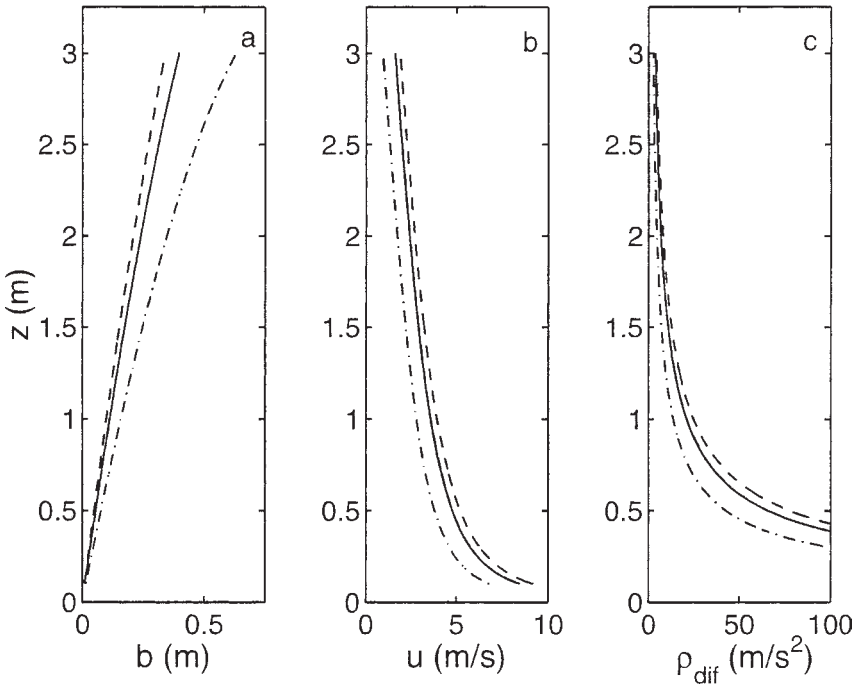

Figure 8. *The effect of the entrainment coefficient, α, on (a) plume width; (b) plume velocity; and (c) plume density difference with $Q = 1\,m^4/s^3$, $d = 0.001\,m$, $u_d = -4\,m/s$, and $n = 500{,}000\,drops/m^3$ (dashed curve: $\alpha = 0.082$; solid curve: $\alpha = 0.093$; dashed/dotted curve: $\alpha = 0.129$).*

decreases to zero near $z = 2\,\text{m}$ for $n = 625{,}000\,\text{drops/m}^3$ and $u_\text{d} = -8.5\,\text{m/s}$. Above this point, the momentum of the droplets overwhelms that of the plume. Of course, the assumptions in the model fail at this point. Nevertheless, this limiting behavior can provide insight into the location of the plume–spray interaction boundary and the relationship between the plume momentum and spray momentum that creates this boundary.

Previous computational work by Nam [8,9] displayed the location of the boundary between the downward moving air entrained by the droplet spray and the upward moving air from the plume. Although the location of this boundary could be identified in only three computer simulations, it is useful to compare results from Nam's simulations to those of this simple model. However, there is a slight difference in the two situations. Nam's results provide the boundary between downward moving air entrained by the droplets and the upward moving plume air, whereas here, the boundary between the downward droplet momentum and that of the plume is

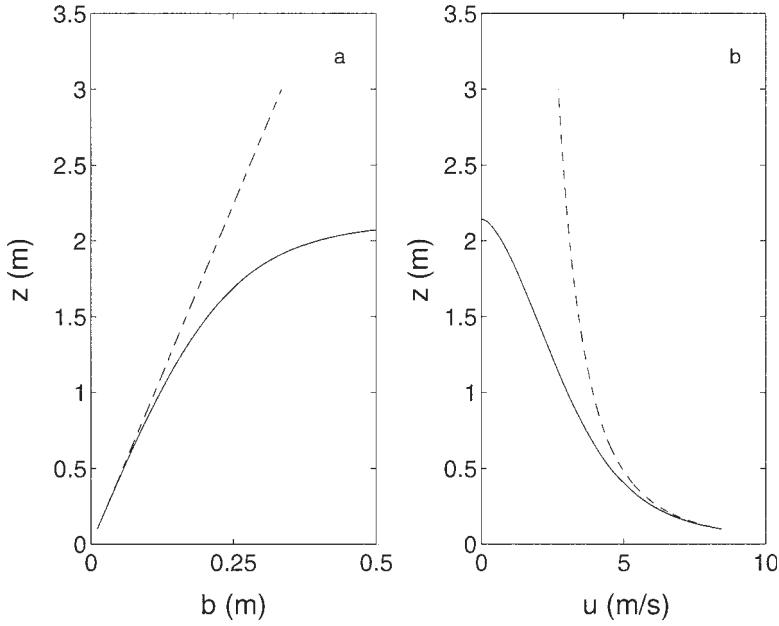

Figure 9. *For large n or u_d, plume velocity goes to zero and plume width extends rapidly. Here $n = 625{,}000$ drops/m^3, $u_d = -8.5$ m/s, $Q = 1$ m^4/s^3, and $d = 0.001$ m (dashed curve: plume with no droplets (Morton solution); solid curve: plume with droplets).*

determined. However, it is reasonable that the location of the two boundaries is similar.

Several simplifications of the spray in Nam's simulations must be made to accommodate the simplified droplet field present in the current model. Droplet velocities were not explicitly stated for all three parameter configurations that Nam used, but recent experimental work in fire sprinklers puts the average vertical droplet velocity at approximately one-half the orifice velocity [11]. For Nam's simulations, orifice velocities of 6.6, 15.6, and 22.0 m/s can be calculated from the given sprinkler flow rates, Q_w, of 1.88, 4.42, and 6.23 L/s and the area of the sprinkler orifice, which was previously reported to be 283.5 mm^2 [16]. This gives values for u_d as 3.3, 7.8, and 11.0 m/s for the three scenarios.

For a sprinkler that is generating uniform droplets of diameter d, the droplet production rate, P_d, is the water flow rate divided by the volume of a droplet so that

$$P_d = \frac{Q_w}{V_d} = \frac{6Q_w}{\pi d^3} \tag{19}$$

Nam reports volumetric median droplet diameters of $d_m = 670\,\mu m$ for the 6.23 L/s flow rate, $d_m = 842\,\mu m$ for the 4.42 L/s flow rate, and $d_m = 1.48\,mm$ for the 1.88 L/s flow rate. The cumulative distribution of the droplets' diameters typical for fire sprinkler sprays is approximated by a lognormal/Rosin Rammler distribution [16]:

$$\mathrm{CVF}(d) = \begin{cases} \dfrac{1}{2\pi}\displaystyle\int_0^d \frac{1}{\sigma d'} e^{(\ln(d'/d_m))^2/2\sigma^2} dd' & (d < d_m) \\ 1 - e^{-\ln 2 (d/d_m)^\gamma} & (d > d_m) \end{cases} \tag{20}$$

where the distribution parameters σ and γ are typically set to 0.5 and 2.43 for fire sprinkler sprays [16]. The derivative of Equation (20) with respect to droplet diameter is the probability density function (pdf) of the volume of the spray as a function of droplet diameter. The resulting pdf can be used to calculate the droplet production rate for a spray with a distribution of droplet sizes

$$P_d = \frac{6Q_w}{\pi}\int_0^{d_{max}} \frac{\mathrm{pdf}(d')}{d'^3} dd' \tag{21}$$

where d_{max} is the maximum diameter of the droplet distribution. The production rate also must be equal to the product of the volumetric flow rate of the spray, Q_s, which includes the drops and the entrained air, and the droplet number density, n. To compute Q_s, the sprinkler spray is assumed to be evenly divided over a finite floor area below the sprinkler, reported as $A = 5.226\,m^2$. The volumetric flow rate of the spray is the product of the coverage area and the spray velocity, which is assumed to be equal to the droplets' velocity, u_d, so that

$$P_d = nAu_d \tag{22}$$

For Nam's simulations, setting the two expressions for the droplet production rate, P_d, equal to one another results in $n = 1.84 \times 10^5\,\mathrm{drops/m^3}$ at 1.88 L/s, $n = 1.02 \times 10^6\,\mathrm{drops/m^3}$ at 4.42 L/s, and $n = 2.03 \times 10^6\,\mathrm{drops/m^3}$ at 6.23 L/s.

For fire sizes, the comparison is more straightforward. Nam uses fires with convective heat release rates of 500, 1000, and 1500 kW. These fire sizes can be related to Q using the equation

$$Q = \frac{Q_c g}{\pi c_p T_1 \rho_1} \tag{23}$$

where Q_c is the convective heat release rate of the fire [12]. In Nam's simulations, Q_c is set at 60 and 40% of the value calculated according to Equation (23) when the sprinkler flow rate is at 4.42 or 6.23 L/s. Nam justified this reduction by the lack of a combustion model in his simulations and visual observations. To account for the finite size of the fire in Nam's model, a virtual origin was back-calculated using Morton's original solution for plume width and the fire radius at $z = 0$ provided by Nam.

A comparison of Nam's simulation results with our model is shown in Figure 10. The nominal boundary for Nam's analysis is shown by the open circles for two combinations of sprinkler flow rates and fire sizes. For the current model, the points calculated for Nam's scenarios are shown as open squares. The curve between the points is calculated by linearly interpolating fire size, sprinkler flow rate, and fire size reduction between the three given combinations that Nam used. The results of this comparison are encouraging. For the largest fire (1500 kW) and a low sprinkler flow rate (1.88 L/s), Nam's simulation shows the fire overwhelming the sprinkler.

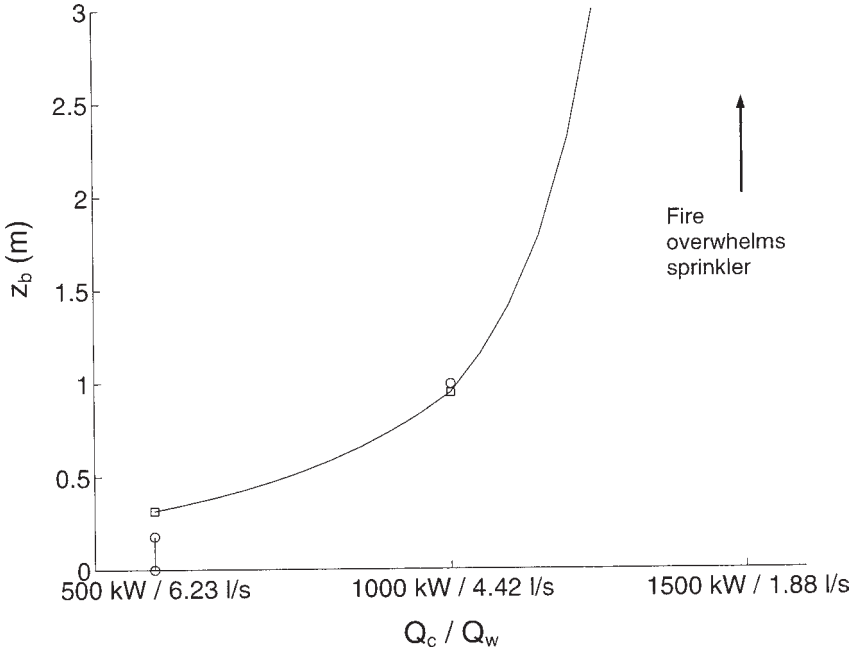

Figure 10. *Predicted location of interaction boundary between upward plume momentum and downward spray momentum. (Open circles: results of Nam [8]; open squares: current model; solid curve: current model interpolation between points.)*

Thus, no boundary is present. This is indicated by the arrow in the upper right corner of Figure 10. For our simple model, there is always a boundary location where the plume velocity is zero, but for this set of parameters, the boundary lies well above the ceiling height that was used in Nam's simulation. Thus, the simple model successfully predicts the fire plume overwhelming the sprinkler's entrained airflow. For the middle scenario with a fire size of 1000 kW and a sprinkler flow rate of 4.42 L/s, neither the sprinkler nor the plume dominate the airflow. Nam's model locates the boundary at 0.99 m above the fire. For the present simple model, the boundary location is at 0.94 m above the fire. For the smallest fire and largest sprinkler flow rate (500 kW, 6.23 L/s), the position of the velocity interface from the simulation cannot be accurately read from Nam's Figure 11 showing velocity vectors, so the vertical line in the lower left corner of Figure 10 indicates the range of possible values, $0 < z_b < 0.17$ m. Matching this scenario's parameters with the current model places the boundary at 0.28 m above the fire. Thus, the present model, which is simple in both physics and implementation, captures much of the behavior shown in the complex computer simulation.

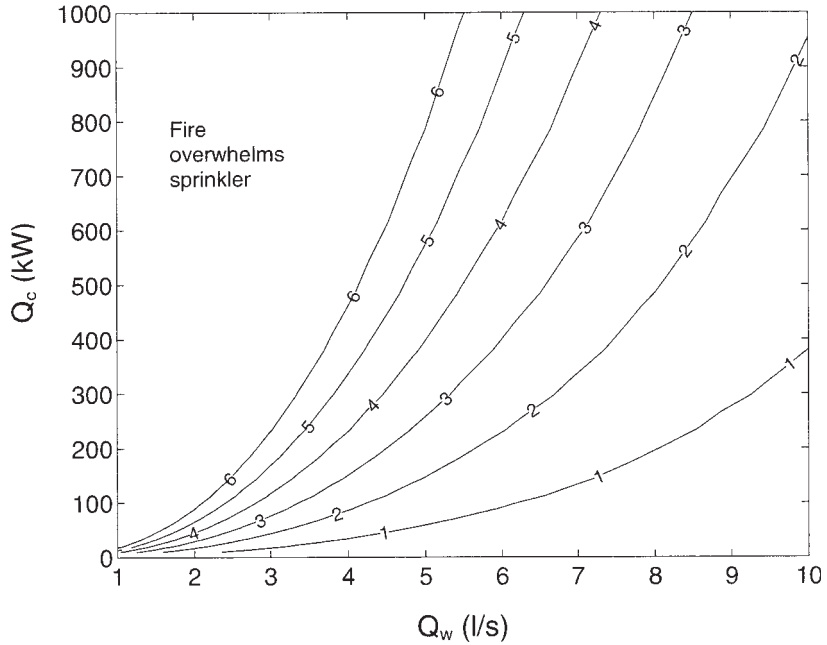

Figure 11. *Contours of the interaction boundary location, z_b (m), with varying fire size, Q_c, and sprinkler flow rate, Q_w ($d = 0.001$ m).*

In a fire suppression application, the variables of interest are a few steps removed from u_d and n. Clearly, fire size and total water flow rate will play an important role in a fire suppression application. Figure 11 shows contours of the interaction boundary location, z_b, calculated for various values of fire size and total flow rate. For this analysis, d was held constant at 0.001 m, a typical value for fire sprinkler droplets [19]. The droplet velocity, u_d, for each flow rate was estimated as one half of the orifice velocity [15], using an orifice of 19 mm. The droplet number density, n, for each flow rate was calculated in the previous manner using the orifice size, droplet diameter, and flow rate through the sprinkler. In addition, to better represent a physical fire, a virtual origin was calculated based on a fire radius of 0.25 m, again based on Morton's original solution for a fire plume.

Figure 11 shows the predictable result that larger fire sizes require larger water flow rates to force the interaction boundary nearer to the fire source. In the upper left region of the figure, the interaction boundary is far enough above typical sprinkler heights that it can be assumed the fire overwhelms the spray. For small sprinkler flow rates in this region, the combination of low flow rate and orifice size causes very low droplet velocities that have little effect on the fire plume. The other regions in the figure emphasize the importance of sprinkler flow rate on fire suppression. For example, doubling the flow rate through the sprinkler from 4 to 8 L/s brings the interaction boundary three times closer to the base of a 500 kW fire.

In the previous figure, u_d and n were both calculated from the sprinkler flow rate. However, if a droplet is considered to be moving at its terminal velocity, which is often the case for sprinkler sprays [13], these parameters vary independently. Consider the case where the flow rate of the sprinkler is fixed and the droplet size is varied (by selecting among sprinklers with different orifices and deflectors resulting in different drop size distributions). In this case, u_d, can be calculated from the droplet terminal velocity in still air, while n is calculated from the sprinkler flow rate and droplet diameter as in previous analyses. Increasing d results in higher u_d due to higher terminal velocity, but smaller n for a fixed volume flow rate of water. Figure 12 shows contours of the interaction boundary location for changing droplet size and fire size while keeping the sprinkler volume flow rate constant at 10 L/s. The location of the boundary is strongly dependent on droplet size for small drops, but less dependent on size for large drops. These results suggest that even though larger droplets survive transit through a fire plume because of their high thermal mass, increasing the droplet size is not effective at preventing fire growth.

Finally, note that it is possible to incorporate a polydisperse spray into the model instead of a monodisperse spray. In this case, Equations (14) and (15) are modified to include a summation over $n_k f_{Dk}$, where k is an index for a

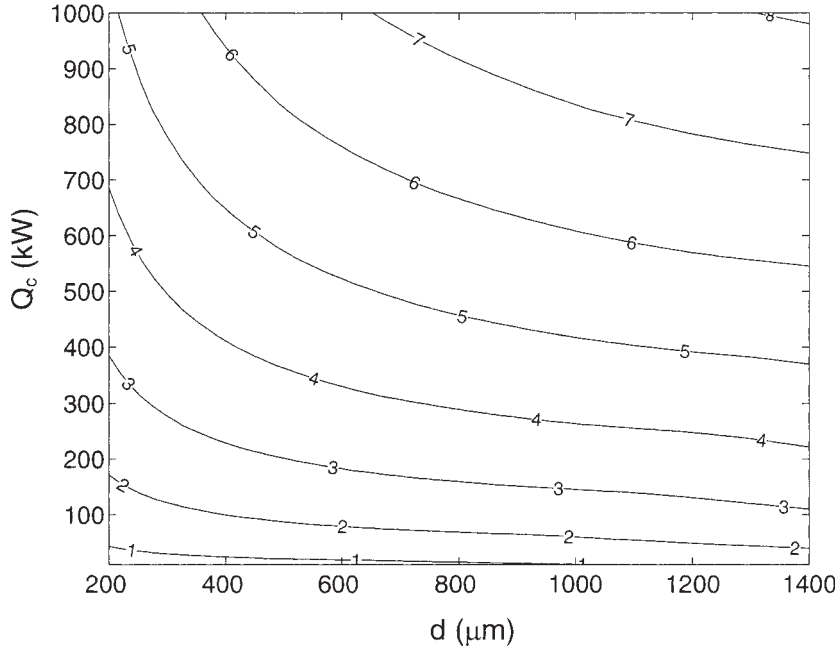

Figure 12. *Contours of the interaction boundary location, z_b (m), with varying d and Q_c, with droplets moving at their terminal velocity ($Q_w = 10$ L/s).*

particular droplet size in a polydisperse droplet size distribution, instead of simply nf_D for a monodisperse distribution. Then a droplet production rate, Equation (21), is calculated for each droplet size, corresponding to index k, in the distribution. However, upon implementation of this approach it becomes clear that a single volumetric diameter could be selected for a monodisperse spray that would give identical results to those for a polydisperse spray. Thus, using a polydisperse spray becomes an unnecessary complication to the model that provides no additional insight into the physics of the interaction between the fire plume and the spray.

CONCLUSIONS

Water is often used in suppression systems due to its advantageous thermal properties [20], making it effective at both cooling burning surfaces and surviving transit through hot plumes. A simple modification of the theory by Morton et al. for buoyant plumes has been made to incorporate a fire sprinkler spray by adding a term in the momentum equation to reflect

the momentum of a uniform disperse droplet field. Of course, actual fire sprinkler sprays do not have uniform droplet fields. The results of this model agree with previous complex CFD simulations even though thermal effects of the droplet phase are not included in the model. Thus, given the agreement of the momentum-based model with previous work, it appears that momentum plays a key role in the interaction between droplet sprays and buoyant plumes. If the upward momentum of the fire plume overwhelms the downward momentum of the spray, the suppression may be ineffective. However, if the downward momentum of the spray, which depends on droplet size, droplet number density, and droplet velocity, overwhelms the upward momentum of the plume, the fire will likely be suppressed. Of course, thermal properties play a role once water reaches the burning surface. However, the separation of fire sprinkler suppression into momentum and thermal effects provides an opportunity for innovative strategies for fire suppression. While evaporation may play a significant role in fire suppression, the momentum of the spray can be used in fire sprinkler design to enhance suppression.

NOMENCLATURE

A = area
A_d = droplet cross-sectional area
b = plume width
C_d = drag coefficient (Equation (8))
c_p = specific heat at constant pressure
d = droplet diameter
d_m = volumetric median droplet diameter
d_{max} = maximum droplet diameter
f_D = drag force (Equation (12))
$\boldsymbol{F}$ = forces
F_b = buoyant force (Equation (5))
F_D = drag force (Equation (6))
Fr = Froude number
g = acceleration of gravity
n = droplet number density
$\boldsymbol{n}$ = unit normal vector
P_d = droplet production rate (Equation (19))
$Q = b^2 ug(\rho_1 - \rho)/\rho_1$
Q_c = convective heat release rate of the fire
Q_s = volumetric flow rate of spray
Q_w = sprinkler flow rate

Re = droplet Reynolds number (Equation (7))
T_1 = ambient air temperature
u = vertical velocity
u_d = vertical droplet velocity
$\boldsymbol{v}$ = air velocity
z = vertical position
z_0 = vertical position of solution starting point
z_b = vertical position of interaction boundary
α = entrainment coefficient
γ = cumulative distribution parameter (Equation (20))
ρ = plume density
ρ_1 = ambient air density
ρ_{dif} = density term (Equation (11))
σ = cumulative distribution parameter (Equation (20))

ACKNOWLEDGMENTS

The first author was supported by a National Science Foundation Graduate Research Fellowship and Northwestern University. Underwriter's Laboratories (UL) provided laboratory facilities for this research. We gratefully acknowledge the support and encouragement of Dr Pravin Gandhi (UL).

REFERENCES

1. Karter, M.J., Fire Loss in the United States During 2002, Report, National Fire Protection Association Quincy MA, Sept. 2003.
2. Cox, G., "Fire Research in the 21st Century," Fire Safety J., Vol. 32, No. 3, 1999, pp. 203–219.
3. Tiezen, S.R., "On the Fluid Mechanics of Fires," Annual Rev. Fluid Mech., Vol. 33, 2001, pp. 67–92.
4. Sirignano, W.A., Fluid Dynamics and Transport of Droplets and Sprays, Cambridge University Press, Cambridge, 1999.
5. Heskestad, G., "Dynamics of the Fire Plume," Phil. Trans. Royal Soc. London, Series A, Vol. 356, No. 1748, 1998, pp. 2815–2833.
6. Morton, B.R., Taylor, G.I. and Turner, J.S., "Turbulent Gravitational Convection from Maintained and Instantaneous Sources," Proc. Royal Soc. London, Vol. 234, No. 1196, 1956, pp. 1–23.
7. Schwille, J.A., Gandhi, P. and Lueptow, R.M., "Fire Plume and Fire Sprinkler Interaction," In: Proceedings of the 8th Annual Fire Suppression and Detection Research Application Symposium, Orlando, FL, 2003, pp. 30–43.
8. Nam, S., "Development of a Computational Model Simulating the Interaction between a Fire Plume and a Sprinkler Spray," Fire Safety J., Vol. 26, No. 1, 1996, pp. 1–33.

9. Nam, S., "Numerical Simulation of Actual Delivered Density of Sprinkler Spray through Fires," Atomization and Sprays, Vol. 4, No. 4, 1994, pp. 385–404.
10. McGrattan, K.B., Baum, H.R., Rehm, R.G., Hamins, A., Forney, G.P., Floyd, J.E., Hostikka, S. and Prasad, K., "Fire Dynamics Simulator (Version 3) – Technical Reference Guide," Technical Report NISTIR 6783, National Institute of Standards and Technology, 2002.
11. Sheppard, D., "Spray Characteristics of Fire Sprinklers," PhD Thesis, Northwestern University, 2002 (see also NIST GCR 02-838).
12. Heskestad, G., "Fire Plumes," In: SFPE Handbook of Fire Protection Engineering, Second Edition, National Fire Protection Association, Quincy, 1995, pp. 2–19.
13. Widmann, J., "Phase Doppler Interferometry Measurements in Water Sprays Produced by Residential Fire Sprinklers," Fire Safety J., Vol. 36, No. 6, 2001, pp. 545–567.
14. Wallis, G., One-dimensional Two Phase Flow, New York, McGraw-Hill, 1969.
15. Sheppard, D. and Lueptow, R.M., "Characterization of Fire Sprinkler Sprays using Particle Image Velocimetry," Atomization and Sprays, Vol. 15, No. 3, 2005, pp. 341–362.
16. Chan, T.S., "Measurements of Water Density and Drop Size Distributions of Selected ESFR Sprinklers," J. Fire Protection Eng., Vol. 6, No. 2, 1994, pp. 79–87.
17. Alpert, R.L., "Calculated Interaction of Sprays with Large-scale Buoyant Flows," J. Heat Transfer, Vol. 106, No. 2, 1984, pp. 310–317.
18. Gebhart, B., Jaluria, Y., Mahajan, R.L. and Sammakia, B., Buoyancy-Induced Flows and Transport, Hemisphere Publishing Corp., New York, 1988, pp. 673–683.
19. You, H., "Investigation of Spray Patterns of Selected Sprinklers with the FMRC Drop Size Measuring System," In: Fire Safety Science-Proceedings of the First International Symposium, Gaithersburg, MD, 1985, pp. 1165–1176.
20. Grant, G., Brenton, J. and Drysdale, D., "Fire Suppression by Water Sprays," Prog. Energy Combustion Sci., Vol. 26, No. 2, 2000, pp. 79–130.